Sharp Downward Branch of the Walker Circulation above the Indian Ocean

Tsubasa Kohyama[1], Tamaki Suematsu[2], and Hiroaki Miura[3]

Key points:

- Processes of realizing the sharp downward branch above the Indian Ocean is discussed by comparing it with the broader Pacific branch.
- Model experiments confirm that the sharp downward branch is sustained by East African topography, rather than radiative cooling.
- Without mountains in East Africa, the eastern Horn of Africa would exhibit wetter and more convective climatology.

Corresponding author: T. Kohyama, Department of Information Sciences, Ochanomizu University, 2-1-1, Otsuka, Bunkyo-ku, Tokyo, 112-8610, Japan. (tsubasa@is.ocha.ac.jp)

[1]Department of Information Sciences,
Ochanomizu University, Tokyo, Japan.

[2]Atmosphere and Ocean Research
Institute, The University of Tokyo, Tokyo,
Japan.

[3]Department of Earth and Planetary
Science, The University of Tokyo, Tokyo,
Japan.

Abstract. Climatological features regarding the sharp downward branch (SDB) of the Walker circulation above the Indian Ocean are comprehensively investigated. Compared to the Pacific downward branch, SDB has two distinctive features: two-peak seasonality and deep subsidence extension. The two weak phases of SDB in boreal spring and fall correspond well to the two rainy seasons at the Eastern Horn of Africa, which is not reproduced well by state-of-the-art global climate models. Unlike the Pacific counterpart, the annual-mean subsidence of SDB extends to the surface, and is supported by horizontal cold advection associated with the Asian Summer Monsoon. Two experiments using a convection-permitting atmospheric general circulation model show that mountains in East Africa, particularly the Ethiopian Highlands, is necessary for the existence of SDB. The dry and clear climate in the Northeast Africa, which is imprinted as a discontinuity of the Intertropical Convergence Zone, is sustained by the East African topography. (149 words)

Index terms: 3319 General circulation

Keywords: Walker Circulation, Intertropical convergence zone, Eastern Horn of Africa

1. Introduction

The Walker circulation is the most prominent planetary-scale tropical atmospheric circulation in the zonal direction [e.g., *Walker*, 1923, 1924; *Bjerknes*, 1969]. It has been understood that, to first order, the vertical motion associated with the Walker circulation consists of upward branches over relatively warm surface (e.g., the warm pool in the western Pacific) and downward branches over relatively cool surface (e.g., the cold tongue in the eastern Pacific) [e.g., *Lau and Yang*, 2003]. In the context of climate variability, the Pacific branches of the Walker circulation have received particular attention, because its interannual fluctuation serves as the atmospheric component of the El Niño Southern Oscillation, the most dominant interannual climate mode on Earth [e.g., *Bjerknes*, 1969].

As a mean state, however, a downward branch of the Walker circulation above the Indian Ocean exhibits stronger subsidence than that of the eastern Pacific. Figure 1a shows the annual-mean equatorial vertical motion calculated by taking the meridional mean over the equatorial region (10°S-10°N). The strong and narrow downward branch stands at the western edge of the Indian Ocean (40°E-60°E), whereas the weak and wide downward branch lies over the eastern Pacific (90°W-150°W). Considering the size of the two oceanic basins, one might find this interbasin contrast counterintuitive. Therefore, in this study, we refer to this downward branch above the Indian Ocean as the Sharp Downward Branch (SDB) of the Walker Circulation, and will investigate its distinctive features and its reason for existence.

One of major implications of SDB is the dry and clear climate at the so-called "Eastern Horn of Africa", whose mean state, annual cycle, variability, and change have long been in-

vestigated in many previous studies [e.g., *Camberlin*, 1995; *Schreck III and Semazzi*, 2004; *Liebmann et al.*, 2014; *Lyon*, 2014; *Tierney et al.*, 2015; *Liebmann et al.*, 2017]. Figures 1b and 1c show the annual mean outgoing longwave radiation (OLR) and precipitation, respectively, over the tropics. The well-known intertropical convergence zone (ITCZ) is typically characterized by the narrow convective band that circles the Earth along the equatorial region. If we carefully look at ITCZ, however, a discontinuity of ITCZ is found near the Eastern Horn of Africa. The location of this ITCZ discontinuity corresponds to that of SDB. Therefore, by investigating SDB, we expect a better understanding of the climatology at the Eastern Horn of Africa, whose annual cycle of precipitation is poorly reproduced by state-of-the-art global climate models [*Tierney et al.*, 2015].

In this study, we shed light on some distinctive features of SDB mainly by comparing it with the Pacific counterpart. We show that the existence of the SDB is sustained by cooling effects originated from the East African topography, rather than radiative cooling. Data and methods are described in the next section. In section 3, we describe the seasonality of SDB, and highlight a role of horizontal cold advection to explain why in some seasons SDB extends to the surface unlike the Pacific downward branch. Then, in section 4, we perform model experiments to identify the East African topography as a necessary condition for the existence of SDB, and discuss implications for the climate at the Eastern Horn of Africa. Conclusions are presented in section 5.

2. Data and Model

2.1. Data

Observed vertical motion, wind, and temperature data are from the European Center for Medium range Weather Forecasting (ECMWF) ERA-Interim reanalysis data [*Dee et al.*, 2011], and the time span used in this study is from 1979 through 2017. Observed OLR data is from the National Oceanic and Atmospheric Administration (NOAA) interpolated OLR [*Liebmann and Smith*, 1996], whose time span used in this study is from June 1974 through December 2018. Observed precipitation data is from the Global Precipitation Climatology Project (GPCP) [*Adler et al.*, 2003], and the time span used in this study is from January 1979 through January 2020. The horizontal resolutions are 3° for vertical motion, wind, and temperature, and 2.5° for OLR and precipitation.

2.2. Atmospheric General Circulation Model (AGCM) experiments

We use the Nonhydrostatic Icosahedral Atmospheric Model (NICAM) [*Tomita and Satoh*, 2004; *Satoh et al.*, 2008, 2014], the version of which used for our experiments is the latest stable version, NICAM16-S [*Kodama et al.*, 2020]. The condensation processes are explicitly calculated using the single moment water 6 microphysics scheme [*Tomita*, 2008a]. Sub-gird scale turbulence is calculated by a modified version of the Mellor-Yamada scheme [*Mellor and Yamada*, 1982; *Nakanishi and Niino*, 2004; *Noda et al.*, 2010]. The radiation model with two stream radiative transfer scheme employs a correlated k-distribution method (mstrnX) [*Sekiguchi and Nakajima*, 2008]. Surface fluxes are calculated with a modified version of the Louis scheme [*Louis*, 1979; *Uno et al.*, 1995]. For the land processes, the minimal advanced treatments of surface interaction

and runoff (MATSIRO) land model [*Takata et al.*, 2003] is used. Orographic gravity wave drag is considered to be sufficiently resolved in our simulations and to be opted out of employing the parameterization for the sub-grid scale orographic gravity wave drag.

The horizontal resolution is approximately 14 km on an icosahedral hexagonal-pentagonal mesh [*Tomita*, 2008b]. A terrain following vertical grid coordinate is employed with the model top of approximately 40 km and 38 vertical layers, whose thickness increases with height. The model time step is 60 seconds. Our simulations are initialized on 00 UTC 28 June 2016 and are integrated for 93 days. Initial conditions of the atmosphere and the ocean are derived from the National Centers for Environmental Prediction (NCEP) Final Operational Model Global Tropospheric Analysis (NCEP-FNL) [*NCEP*, 2015]. Time evolution of the sea surface temperature is prescribed externally from the interpolation of the NCEP-FNL data at 00 UTC on each day. To mitigate the effect of the model bias over land, the initial conditions of the land surface are taken from the monthly climatology derived from the last 5 years of a 10-year simulation of NICAM at 220 km horizontal resolution following *Kodama et al.* [2015, 2020]. Because it takes approximately 45 days for the values of vertical motions to converge to realistic climatological values, the first 63 days of the integrations are taken as the spin-up period, and the last 30 days of the integrations starting from 1 September 2016 are analyzed in this study.

3. Distinctive features of the Sharp Downward Branch (SDB)

In this section, we first overview the seasonality of SDB and the consistency with the local rainy seasons. Then, from the energetic viewpoint, we explain why SDB can penetrate the lower tropospheric boundary layer and extends to the surface.

3.1. Two-peak seasonality of SDB

SDB exhibits two-peak seasonal variability in its strength of the subsidence. The left panels of Fig. 2 shows the monthly-mean equatorial vertical motion. SDB exhibits moderate subsidence from January through March, almost disappears from April through May, reaches its strongest phase from June through September, and becomes weak from October through December.

The phase of this two-peak seasonality corresponds well to the annual precipitation cycle of the Eastern Horn of Africa, where two rainy seasons are known to exist. In this region, the term "Long Rains" denotes the longest and wettest rainy season that lasts from April through May, and the term "Short Rains" denotes the shorter and drier rainy season that peaks in October. Presumably, the lack of this seasonality in state-of-the-art GCMs [*Tierney et al.*, 2015] is inseparable from the reproducibility of the seasonal variability of SDB.

3.2. "Subsidence extension" of SDB to the surface and its energetic constraint

One of the essential features of SDB is that the subsidence reaches the surface in the annual-mean basis, which is not the case for the Pacific downward branch (Fig. 1a). In SDB, horizontal advection plays a key role for lower tropospheric atmospheric subsidence to extend to the surface. The right panels of Fig. 2 shows the mean horizontal heat advection, which is defined as the inner product of mean horizontal wind and the horizontal gradient of mean temperature. Our definition of the mean horizontal advection does not take eddy heat transport into account.

The strongest subsidence observed from June through September is supported by the mean horizontal advection. In general, adiabatic heating of large-scale downward motions is needed to balance radiative cooling in the tropics, and this energy budget is mostly true for the Walker circulation as well [*Veiga et al.*, 2011]. As described in the previous paragraph, however, it is not the case for SDB. The contribution from the horizontal temperature advection makes this "subsidence extension" be a distinctive feature that can be observed particularly in this region.

This "subsidence extension" serves as a good example where interscale interaction plays a fundamental role in downward branches, in addition to convective upward branches, to realize the large-scale atmospheric circulation in the current tropical climate. Specifically, the narrowly localized downward branch above the Indian Ocean is realized with a help of interactions between large-scale motions and smaller disturbances in horizontal scales where weak temperature gradient approximation [*Sobel et al.*, 2001] is no longer valid.

A plausible hypothesis about the origin of this horizontal cold advection is that, because horizontal winds associated with the monsoon of South Asia prevails in this region, the lower troposphere is cooled more efficiently, with a help of a large land-sea contrast of temperature, than in the Pacific. Presumably, this cooling effect would drag down the Walker Circulation to the surface. This notion is also consistent with the disappearance of SDB from April through May, because this season is the period when the Asian summer monsoon are weakened to switch its direction before the onset of the strong Somali jet in early June [e.g., *Findlater*, 1969]. This hypothesis will be revisited in the next section.

4. The role of the East African topography for sustaining SDB

Though we have identified the cause of strong subsidence in the lower troposphere, it remains unclear what makes the subsidence in SDB so strong that SDB penetrates the entire troposphere in the vertical direction. Therefore, in this section, we perform model experiments to highlight the role of topography for sustaining SDB. Some implications for the climate of the Eastern Horn of Africa are also discussed.

4.1. Model experiments with flat East African topography

Our experiments are inspired by *Naiman et al.* [2017], who showed, in an interesting way, that topography can play major roles in determining the tropical circulation. Using an Earth System Model (ESM), Geophysical Fluid Dynamics Laboratory (GFDL)-ESM2M, they performed an experiment called "Pancake", in which they removed all the topography on Earth and simulated the air-sea coupled system with flat lands. Because SDB disappears in their "Pancake" run, we have hypothesized that, by flattening topography in narrower regions, it is possible to pinpoint the location of mountains that directly contribute to the realization of SDB.

In this study, in addition to a control run, we arrange two additional AGCM experiments where the East African topography is regionally flattened. The first experiment is named "Flat Ethiopia (FET)", in which the altitudes are set to be 1 meter for all the grids in Ethiopian Highlands (3°N-16°N, 34°E-43°E) (Fig. 3a, top). The second experiment is named "Flat East Africa (FEA)", in which the altitudes are set to be 1 meter over the entire East African region (10°S-10°N, 10°S-10°N) (Fig. 3a, bottom).

The sensitivity experiment reveals that the East African topography, especially the Ethiopia Highlands, is a necessary condition for the existence of SDB. Figure 3b shows the monthly-mean equatorial vertical motion in September 2016 from observations and three model experiments, i.e., control, FET, and FEA. The control run simulates the observed vertical motion associated with the Walker circulation well, so it is justified to investigate SDB using this AGCM. In the FET run, the subsidence extension of SDB in the lower troposphere is weakened. In the FEA run, SDB disappears almost entirely through the troposphere.

At least two physical processes can potentially explain why SDB disappears once the topographic forcing is lost. One mechanism is that, without the topography in these regions, the Somali jet are distracted from its usual pathway, which weakens the cooling effect of horizontal advection. This mechanism is consistent with the aforementioned evidence that the Somali jet cools the lower troposphere in the SDB region. Another possible mechanism is that, the lack of turbulence generated by mountain waves suppresses vertical mixings. Because the lower troposphere generally has lower potential temperature than the upper troposphere, the reduction of vertical heat exchange weakens the subsidence of upper tropospheric air.

4.2. Implications for the climate of the Eastern Horn of Africa

Without the East African topography, the dry and clear climate at the Eastern Horn of Africa becomes wetter and more convective. Figure 4 shows the monthly-mean OLR and precipitation near SDB. By virtue of the high-resolution convection-permitting model that explicitly calculates the vertical motion, the control run reproduces both OLR and

precipitation well, particularly the discontinuity of ITCZ. In the FET and FEA runs, as the East African topography is flattened, the discontinuity of ITCZ disappears, which makes the Eastern Horn of Africa be covered by ITCZ. Only in the FET run, clouds and moisture avoid the mountains located to the south of the Ethiopian Highlands, which are not flattened in this particular experiment.

Both local processes and remote forcings can contribute to the "closing" of the ITCZ discontinuity in the FET and FEA runs. Locally, the lack of SDB enhances convection above the Eastern Horn of Africa. This enhancement is due to the reduction of large-scale atmospheric subsidence that relatively moistens local air and favors upward motion. In addition to this local instability effect, clouds and moist air, which are advected remotely by trade winds, are also allowed to enter the Eastern Horn of Africa from the Indian Ocean, because topographic obstacles do not exist.

5. Summary and Discussions

We have reconsidered the climatology of the Walker circulation by focusing on its sharp downward branch, which we refer to as SDB, observed at the western edge of the Indian Ocean (Fig. 1). The following two observed features of SDB are distinctive compared to the Pacific downward branch. The first feature is the two-peak seasonality (Fig. 2a). The two weak phases of SDB, one in boreal spring and the other in boreal fall, correspond well to the two rainy seasons at the Eastern Horn of Africa, which is not reproduced well by state-of-the-art GCMs. The other distinctive feature is that the annual-mean subsidence of SDB reaches the surface (Fig. 1a). This "subsidence extension" appears to be sustained by horizontal cold advection associated with the Asian Summer Monsoon (Fig. 2b).

Two AGCM experiments show that the East African topography determines the strength of SDB (Fig. 3). In the FET experiment, where the Ethiopian Highlands is flattened, the lower troposphere does not subside any longer. In the FEA experiment, where the East African mountains are broadly flattened, SDB becomes as weak as the Pacific downward branch throughout the entire troposphere. Based on previous studies on the Pacific downward branch [*Veiga et al.*, 2011], the remaining weak downward motion is presumably induced by radiative cooling.

These results leads to a robust conclusion that the East African topography, particularly the Ethiopian Highlands, is necessary for the existence of SDB. Based on this conclusion, we hypothesize two roles of topography in this region. The first role is to force Asian Monsoon to flow in the cross-equatorial direction. This meridional flow, such as the Somali Jet, transports relatively cool extratropical air into the tropics, and drags down the lower troposphere. The other role is to generate mountain waves in response to large-scale circulation. The steady vertical mixings enhance vertical heat exchange to cool the upper troposphere, which makes SDB rigid. Assuming this mechanism, climate variability of SDB could also be understood based on interscale interactions between macroscopic large-scale circulation and microscopic mountain waves. Further process studies are needed to improve the robustness of these physical processes.

An important implication of our conclusion is that the dry and clear climate at the Eastern Horn of Africa is sustained by the East African topography (Fig. 4). As a local effect, the large-scale subsidence associated with SDB suppresses the local convection by drying the environment and by suppressing upward motion. At the same time, the high

mountains in the East Africa, particularly the Ethiopian Highlands, serves as obstacles that prevents clouds and moist air from stepping onto the African continent. Because both of these local and remote processes are consistent with the essentiality of the East African topography, it remains to be an open question which process serves as the dominant cause of the ITCZ discontinuity.

Acknowledgments. This study is based on the ERA-Interim dataset available online at `https://apps.ecmwf.int/datasets/data/interim-full-moda/levtype=pl/`, the NOAA interpolated OLR dataset available online at `https://psl.noaa.gov/data/gridded/data.interp_OLR.html`, and the GPCP dataset available online at `https://psl.noaa.gov/data/gridded/data.gpcp.html`. The first author is supported by the Japan Society for the Promotion of Science (JSPS)-Kakenhi Grant Number 19K23460 and 20K14554. The third author is supported by JSPS-Kakenhi Grant Number 16H04048. The numerical computations using NICAM is performed on a super computer, Oakforest-PACS.

References

Adler, R. F., G. J. Huffman, A. Chang, R. Ferraro, P.-P. Xie, J. Janowiak, B. Rudolf, U. Schneider, S. Curtis, D. Bolvin, et al. (2003), The version-2 global precipitation climatology project (gpcp) monthly precipitation analysis (1979–present), *J. Hydrometeor.*, *4*(6), 1147–1167.

Bjerknes, J. (1969), Atmospheric teleconnections from the equatorial Pacific, *Mon. Wea. Rev.*, *97*(3), 163–172.

Camberlin, P. (1995), June-september rainfall in north-eastern Africa and atmospheric signals over the tropics: A zonal perspective, *International Journal of Climatology*, *15*(7), 773–783.

Dee, D. P., S. M. Uppala, A. Simmons, P. Berrisford, P. Poli, S. Kobayashi, U. Andrae, M. Balmaseda, G. Balsamo, d. P. Bauer, et al. (2011), The ERA-Interim reanalysis: Configuration and performance of the data assimilation system, *Quart. J. Roy. Meteor. Soc.*, *137*(656), 553–597.

Findlater, J. (1969), A major low-level air current near the Indian Ocean during the northern summer, *Quarterly Journal of the Royal Meteorological Society*, *95*(404), 362–380.

Kodama, C., Y. Yamada, A. T. Noda, K. Kikuchi, Y. Kajikawa, T. Nasuno, T. Tomita, T. Yamaura, H. G. Takahashi, M. Hara, et al. (2015), A 20-year climatology of a NICAM AMIP-type simulation, *Journal of the Meteorological Society of Japan. Ser. II*, *93*(4), 393–424.

Kodama, C., T. Ohno, T. Seiki, H. Yashiro, A. T. Noda, M. Nakano, Y. Yamada, W. Roh, M. Satoh, T. Nitta, D. Goto, H. Miura, T. Nasuno, T. Miyakawa, Y.-W. Chen, and M. Sugi (2020), The non-hydrostatic global atmospheric model for cmip6 highresmip simulations (nicam16-s): Experimental design, model description, and sensitivity experiments, *Geoscientific Model Development Discussions*, *2020*, 1–50, doi: 10.5194/gmd-2019-369.

Lau, K., and S. Yang (2003), Walker circulation, *Encyclopedia of atmospheric sciences*, pp. 2505–2510.

Liebmann, B., and C. A. Smith (1996), Description of a complete (interpolated) outgoing longwave radiation dataset, *Bull. Amer. Meteor. Soc.*, *77*(6), 1275–1277.

Liebmann, B., M. P. Hoerling, C. Funk, I. Bladé, R. M. Dole, D. Allured, X. Quan, P. Pegion, and J. K. Eischeid (2014), Understanding recent eastern Horn of Africa rainfall variability and change, *Journal of Climate*, *27*(23), 8630–8645.

Liebmann, B., I. Bladé, C. Funk, D. Allured, X.-W. Quan, M. Hoerling, A. Hoell, P. Peterson, and W. M. Thiaw (2017), Climatology and interannual variability of boreal spring wet season precipitation in the eastern horn of africa and implications for its recent decline, *Journal of Climate*, *30*(10), 3867–3886.

Louis, J.-F. (1979), A parametric model of vertical eddy fluxes in the atmosphere, *Boundary-Layer Meteorology*, *17*(2), 187–202.

Lyon, B. (2014), Seasonal drought in the Greater Horn of Africa and its recent increase during the March–May long rains, *Journal of Climate*, *27*(21), 7953–7975.

Mellor, G. L., and T. Yamada (1982), Development of a turbulence closure model for geophysical fluid problems, *Reviews of Geophysics*, *20*(4), 851–875.

Naiman, Z., P. J. Goodman, J. P. Krasting, S. L. Malyshev, J. L. Russell, R. J. Stouffer, and A. T. Wittenberg (2017), Impact of mountains on tropical circulation in two Earth system models, *Journal of Climate*, *30*(11), 4149–4163.

Nakanishi, M., and H. Niino (2004), An improved Mellor–Yamada level-3 model with condensation physics: Its design and verification, *Boundary-layer meteorology*, *112*(1), 1–31.

NCEP (2015), NCEP GDAS/FNL 0.25 degree global tropospheric analyses and forecast grids.

Noda, A. T., K. Oouchi, M. Satoh, H. Tomita, S.-i. Iga, and Y. Tsushima (2010), Importance of the subgrid-scale turbulent moist process: Cloud distribution in global cloud-resolving simulations, *Atmospheric Research*, *96*(2-3), 208–217.

Satoh, M., T. Matsuno, H. Tomita, H. Miura, T. Nasuno, and S.-i. Iga (2008), Nonhydrostatic icosahedral atmospheric model (NICAM) for global cloud resolving simulations, *Journal of Computational Physics*, *227*(7), 3486–3514.

Satoh, M., H. Tomita, H. Yashiro, H. Miura, C. Kodama, T. Seiki, A. T. Noda, Y. Yamada, D. Goto, M. Sawada, et al. (2014), The non-hydrostatic icosahedral atmospheric model: Description and development, *Progress in Earth and Planetary Science*, *1*(1), 18.

Schreck III, C. J., and F. H. Semazzi (2004), Variability of the recent climate of eastern Africa, *International Journal of Climatology: A Journal of the Royal Meteorological Society*, *24*(6), 681–701.

Sekiguchi, M., and T. Nakajima (2008), A k-distribution-based radiation code and its computational optimization for an atmospheric general circulation model, *Journal of Quantitative Spectroscopy and Radiative Transfer*, *109*(17-18), 2779–2793.

Sobel, A. H., J. Nilsson, and L. M. Polvani (2001), The weak temperature gradient approximation and balanced tropical moisture waves, *Journal of the atmospheric sciences*, *58*(23), 3650–3665.

Takata, K., S. Emori, and T. Watanabe (2003), Development of the minimal advanced treatments of surface interaction and runoff, *Global and planetary Change*, *38*(1-2),

209–222.

Tierney, J. E., C. C. Ummenhofer, and P. B. deMenocal (2015), Past and future rainfall in the Horn of Africa, *Sci. Adv.*, *1*(9), e1500,682.

Tomita, H. (2008a), New microphysical schemes with five and six categories by diagnostic generation of cloud ice, *Journal of the Meteorological Society of Japan. Ser. II*, *86*, 121–142.

Tomita, H. (2008b), A stretched icosahedral grid by a new grid transformation, *Journal of the Meteorological Society of Japan. Ser. II*, *86*, 107–119.

Tomita, H., and M. Satoh (2004), A new dynamical framework of nonhydrostatic global model using the icosahedral grid, *Fluid Dynamics Research*, *34*(6), 357.

Uno, I., X.-M. Cai, D. Steyn, and S. Emori (1995), A simple extension of the Louis method for rough surface layer modelling, *Boundary-layer meteorology*, *76*(4), 395–409.

Veiga, J. A. P., V. B. Rao, and S. H. Franchito (2011), Annual mean analysis of the tropical heat balance and associations with the Walker circulation, *Revista Brasileira de Meteorologia*, *26*(1), 01–08.

Walker, G. T. (1923), Correlations in seasonal variation of weather, VIII: A preliminary study of world weather, *Mem. Indian Meteorol. Dep.*, *24*, 75–131.

Walker, G. T. (1924), Correlations in seasonal variations of weather, IX: A further study of world weather, *Mem. Indian Meteorol. Dep.*, *24*, 275–332.

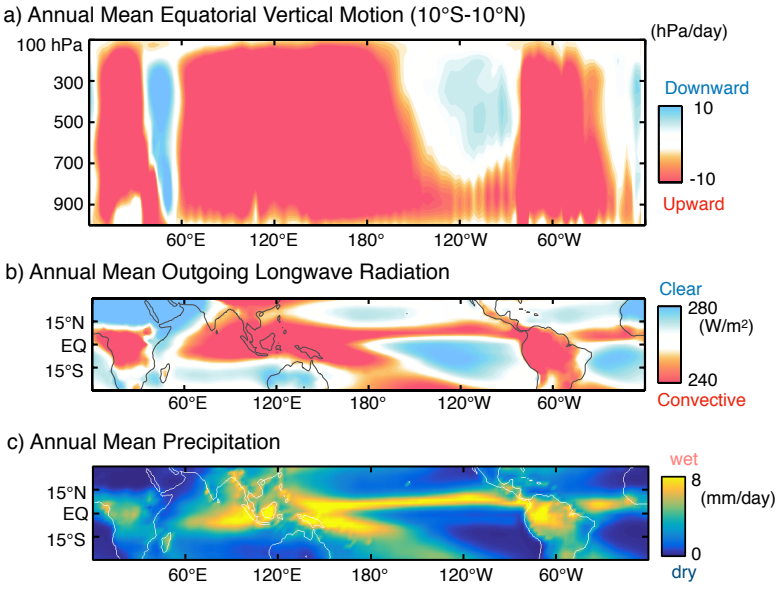

Figure 1. (a): Observed annual-mean vertical motion averaged meridionally over the equatorial region (10°S-10°N). (b): Observed annual-mean outgoing longwave radiation (OLR). (c): Observed annual-mean precipitation.

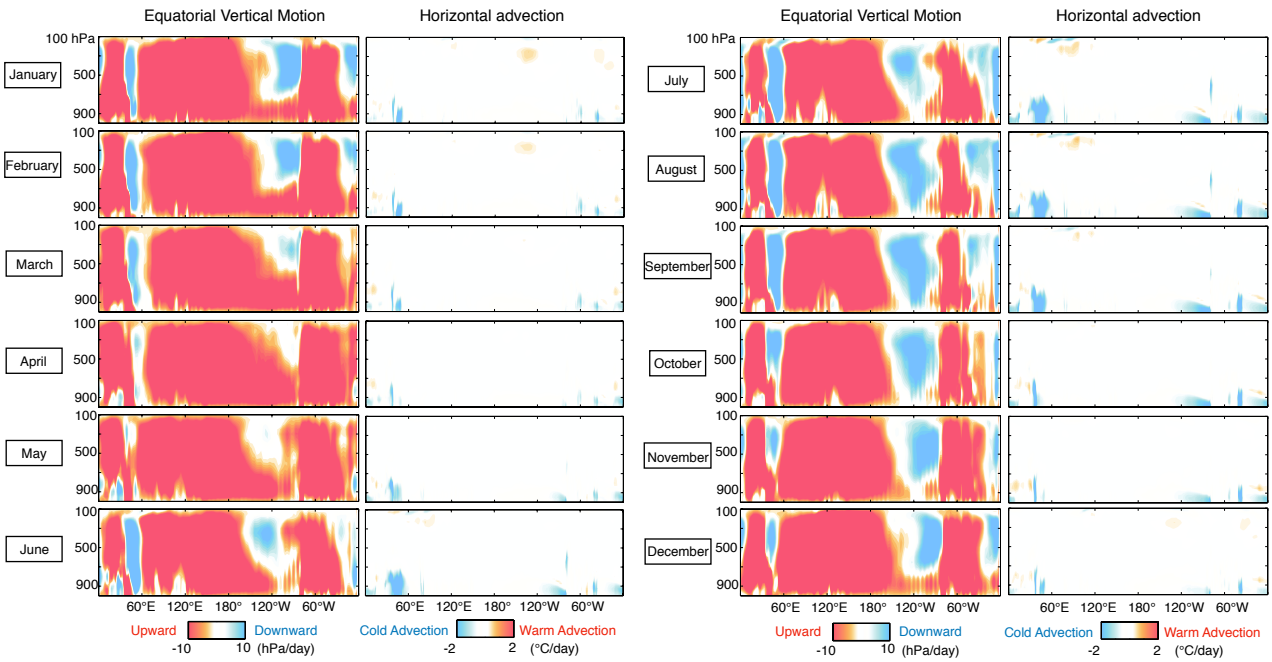

Figure 2. Left columns, As in Fig. 1a, but monthly mean values for each month. Right columns, As in right, but for mean horizontal advection defined as the inner product of mean horizontal wind and the horizontal gradient of mean temperature.

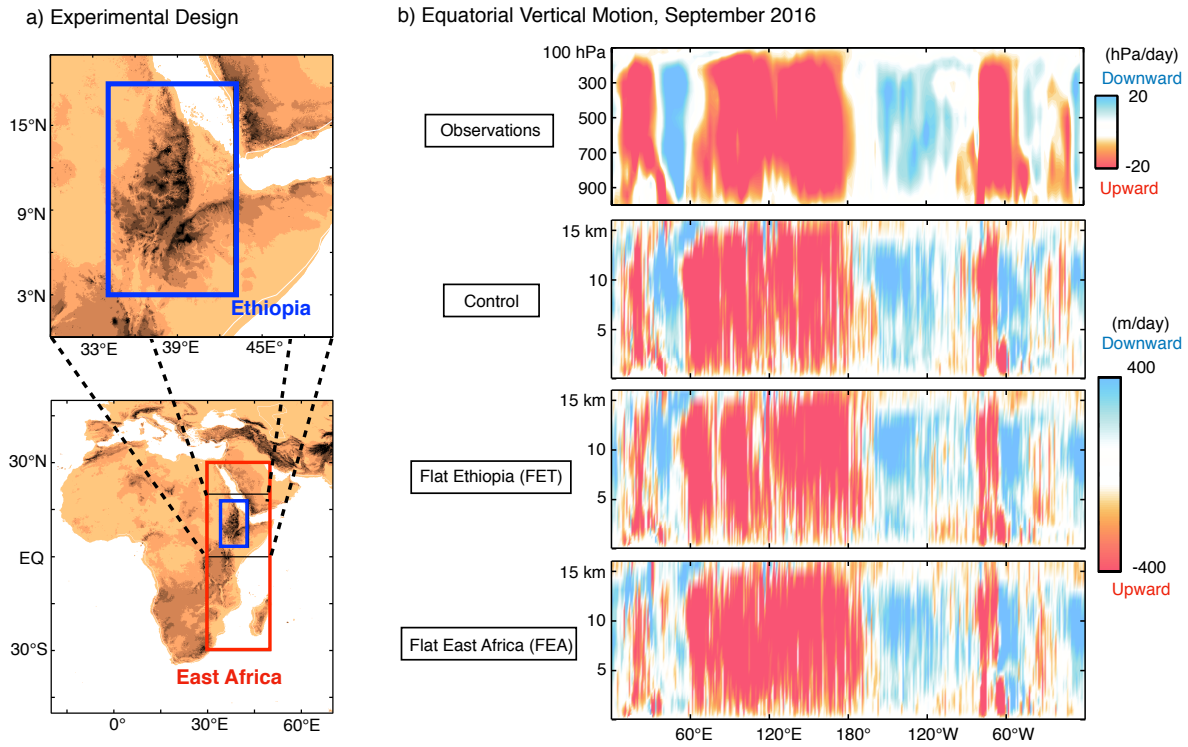

Figure 3. (a): Top, North-east African topography. Blue box shows the Ethiopian Highlands region (3°N-16°N, 34°E-43°E). Bottom, As in top, but for the entire African continent. Red box shows the East African region (10°S-10°N, 10°S-10°N). (b): As in Fig. 1a, but for one-month mean values calculated for September 2016 based on observations, the control, Flat Ethiopia (FET), and Flat East Africa (FEA) experiments in this order from the top panel. In the FET experiment, the topography in the Ethiopian Highlands region is flattened. In the FEA experiment, the topography in the East African region is flattened.

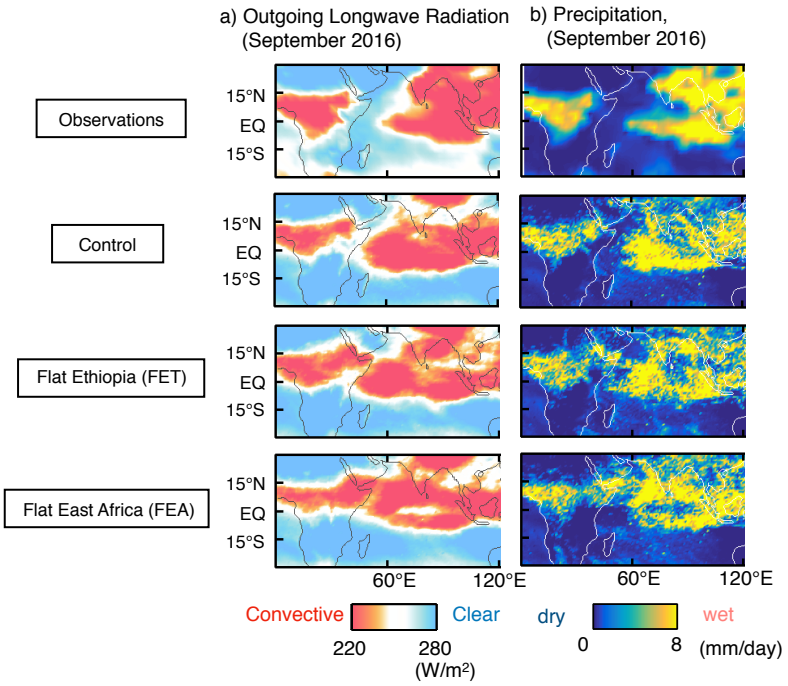

Figure 4. (a): As in Fig. 3b, but for OLR. (b): As in Fig. 3b, but for precipitation.